REPORT DOCUMENTATION PAGE

AFRL-SR-BL-TR-00-0338
AFRL-SR-BL-TR-00-0339
~~0338~~

1. REPORT DATE (DD-MM-YYYY)	2. REPORT TYPE	6/1/96 to 5/31/99
20/07/00	Final Performance Report	

4. TITLE AND SUBTITLE

Visual guided navigation.

5a. CONTRACT NUMBER

5b. GRANT NUMBER
F49620-96-1-0250

5c. PROGRAM ELEMENT NUMBER
F49620-94-1-0214

6. AUTHOR(S)
Martin S. Banks

5d. PROJECT NUMBER
3484, 2313

5e. TASK NUMBER
YS, AS

5f. WORK UNIT NUMBER

7. PERFORMING ORGANIZATION NAME(S) AND ADDRESS(ES)

School of Optometry, 360 Minor, Univ of Calif, Berkeley, Berkeley, CA 94720-2020

8. PERFORMING ORGANIZATION REPORT NUMBER

9. SPONSORING / MONITORING AGENCY NAME(S) AND ADDRESS(ES)

AFOSR/NL
801 North Randolph Street
Arlington, VA 22203-1977

10. SPONSOR/MONITOR'S ACRONYM(S)

11. SPONSOR/MONITOR'S REPORT NUMBER(S)

12. DISTRIBUTION / AVAILABILITY STATEMENT

APPROVED FOR PUBLIC RELEASE: DISTRIBUTION UNLIMITED

20000804 211

13. SUPPLEMENTARY NOTES

14. ABSTRACT The problem of visual space perception is the recovery of the location, shape, size, and orientation of objects in the environment from the pattern of light reaching the eyes. Similarly, the problem of visual navigation is the recovery of an observer's self-motion with respect to the environment from the moving pattern of light reaching the eyes and the complex of extra-retinal signals including eye-muscle, neck-muscle, and vestibular signals. During the last two and a half years, we continued our theoretical and experimental investigations of human visual navigation and space perception. Our accomplishments include several publications in referred scientific journals, the completion of a rotating chair apparatus for use in studying visual-vestibular interactions, and the development of numerous software tools for the control of psychophysical experimentation including graphic display, control of external devices, and analysis of experimental data. These accomplishments are relevant to several aspects of the military aviation mission including 1) how the use of synthetic visual displays (virtual reality in the advanced cockpit, night-vision goggles, etc.) will affect perceived self-motion and spatial orientation, 2) how extra-retinal signals that occur in high-performance flying will affect perceived self-motion and orientation and 3) what visual properties synthetic displays will have to have to prevent or minimize spatial disorientation illusions.

15. SUBJECT TERMS
Visaul, Navigation

16. SECURITY CLASSIFICATION OF:			17. LIMITATION OF ABSTRACT	18. NUMBER OF PAGES	19a. NAME OF RESPONSIBLE PERSON
a. REPORT	b. ABSTRACT	c. THIS PAGE			Martin S. Banks
Unclas	Unclas	Unclas		20	19b. TELEPHONE NUMBER (include area code) (510) 642-9341

Final Technical Report

Visual Navigation and Space Perception

Martin S. Banks
School of Optometry and Vision Science Program
University of California, Berkeley

Progress Report

"Visual Navigation & Space Perception", M.S. Banks

During the last two and a half years, we worked on two general problems: Surface perception and heading perception. In this progress report, we review the work leading up to our current work (thus some of the material appeared on last year's progress report) and then we discuss the work completed this past year.

1. Surface Perception

The problem of visual space perception is the recovery of the location, shape, size, and orientation of objects in the environment from the pattern of light reaching the eyes. The visual system uses disparities between the two retinal images to glean information about the 3-D layout of the environment. In the past five years, we have been investigating how disparity is used to recover surface orientation. Most of the work has concerned determining the slant of an isolated surface rotated about a vertical axis. This problem is interesting because the pattern of disparities depends not only on slant, but also on location relative to the head (Ogle, 1950).

The first part of this section is basically the same as last year's progress report because we need to explain the background to the work we accomplished during the two and a half year grant period. If you have already read this background material from previous progress reports, you can skip ahead to page 5.

Figure 1 depicts the geometry for binocular viewing of a vertical plane. The objective gaze-normal surface is the plane perpendicular to the cyclopean line of sight. The slant S is the angle by which the plane of interest is rotated about a vertical axis from the gaze-normal surface.

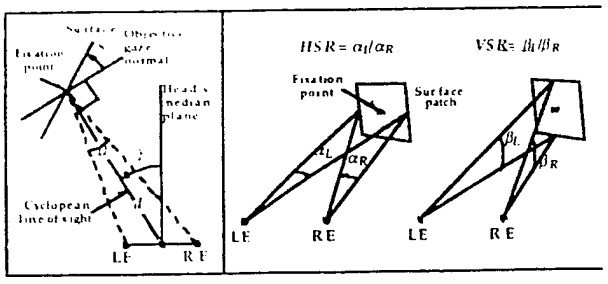

Figure 1. Binocular viewing geometry. See text.

What signals are available for slant estimation? One important signal is horizontal disparity. For a smooth surface slanted about a vertical axis, the horizontal disparity pattern can be represented locally by the horizontal size ratio (*HSR*; Figure 1), the ratio of horizontal angles the patch subtends in the left and right eyes (Rogers & Bradshaw, 1993). Changes in *HSR* produce obvious and immediate changes in perceived slant, so this signal must be involved in slant estimation. However, *HSR* by itself is ambiguous. To illustrate the ambiguity, Figure 2 shows several surface patches that give rise to *HSR*s of 1 and 1.04. For each *HSR* value, there is an infinitude of possible slants depending on the surface's location. Clearly, the measurement of *HSR* alone does not allow an unambiguous estimate of the surface's orientation nor do any other descriptions of horizontal disparity (Longuet-Higgins, 1982). A main purpose of our work has been to determine what other signals are used, in combination with horizontal disparity, by the visual system and to determine how those signals are combined to determine surface slant.

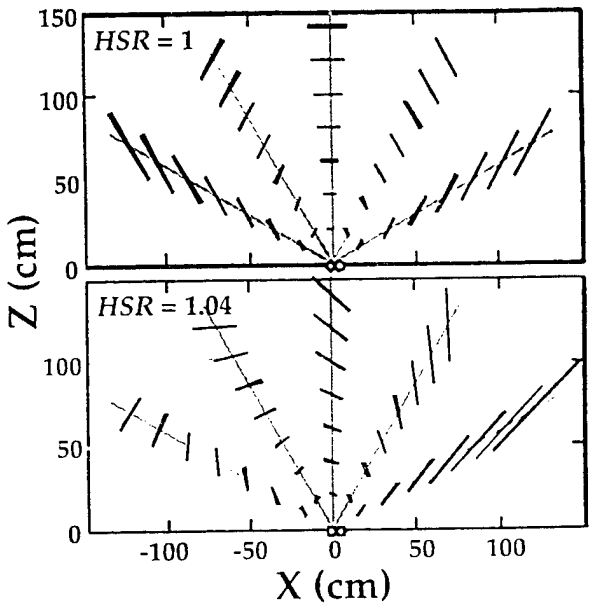

Figure 2. Ambiguity of *HSR*. Plan view with the abscissa representing lateral position and the ordinate forward position. The line segments represent surface patches that give rise to *HSR* = 1 (upper panel) and *HSR* = 1.04 (lower panel).

Another potentially useful signal is vertical disparity which can be represented by the vertical size ratio (*VSR*; Figure 1), the ratio of vertical angles subtended by a surface patch in the left and right eyes. *VSR* varies with the location of a surface patch relative to the head, but does not vary with surface slant (Gillam & Lawergren, 1983). The gray circles in Figure 3 show the *VSR* at various locations in the visual plane. Another

signal is the rate of change in *VSR* with azimuth ($\partial VSR/\partial\gamma$); this signal depends strongly on distance and less so on slant.

Other useful signals are provided by sensed eye position. Ignoring torsion, each eye has one degree of freedom in the visual plane. We can thus represent binocular eye position by two values, γ and μ, the version and vergence of the eyes (Figure 1).

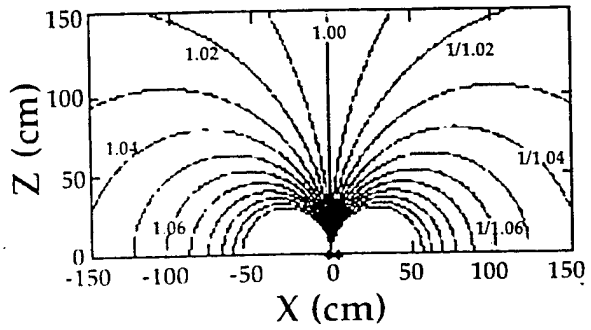

Figure 3. Iso*VSR* contours. Plan view. Abscissa represents lateral position and ordinate forward position. Each contour represents the regions in space for which *VSR* is constant; each contour represents a different *VSR*.

Finally, useful slant information can be gleaned from nonstereoscopic signals such as the texture gradient created by projection onto the retinae of surfaces with statistically regular textures (Cutting & Millard, 1984; Buckley & Frisby, 1993; Cumming et al, 1993). Such cues were present in older stereoscopic work using real objects (e.g., Ogle, 1938; Gillam et al, 1988). In more recent work with computer displays, there is still generally a perspective cue that indicates that the surface is frontoparallel to the head (e.g., Rogers & Bradshaw, 1995; Howard & Kaneko, 1994). Neither the slant specified by a given texture gradient nor the uncertainty of the estimation varies with distance or azimuth (Sedgwick, 1986; Backus et al, 1999).

An unambiguous estimate of slant can be obtained from various combinations of the above-mentioned signals. For example, slant can in principle be estimated from *HSR* and sensed eye position (Ogle, 1950; Foley, 1980). From Backus et al (1999):

$$\hat{S} = \tan^{-1}\left(\frac{1}{\mu}\ln HSR - \tan\gamma\right). \qquad (1.1)$$

The estimates of μ and γ ($\hat{\mu}$ and $\hat{\gamma}$) are presumably derived from extra-retinal, eye-position signals. Correcting *HSR* via eye position has the important consequence of compensating for the changes in binocular viewing geometry that occur with changes in distance and azimuth (Kaneko & Howard, 1996; Ogle, 1950).

Slant can also be estimated from retinal-image information alone (Gårding, *et al.*, 1995; Gillam & Lawergren, 1983; Koenderink & van Doorn, 1976; Mayhew & Longuet-Higgins, 1982). From Backus et al:

$$\hat{S} = -\tan^{-1}\left(\frac{1}{\mu}\ln\frac{HSR}{VSR}\right) \qquad (1.2)$$

where μ can be measured from retinal image properties alone. In the terminology of Gårding et al (1995), μ "normalizes" the slant (scales *HSR* for changes due to viewing distance) and *VSR* "corrects" the slant (corrects *HSR* for changes due to azimuth).

In summary, certain subsets of signals allow unambiguous estimation of slant and we can summarize them with three calculations (Banks & Backus, 1998a): (1) slant estimation from *HSR* and eye position ($\hat{S}_{HSR,EP}$), (2) slant estimation from *HSR* and *VSR* ($\hat{S}_{HSR,VSR}$), and (3) slant estimation from nonstereoscopic cues such as perspective ($\hat{S}_{p}$).

In natural viewing, the slant estimates derived from these three methods should on average agree. However, each signal measurement is subject to error, so even in natural viewing, the estimates will differ. Because a surface can only have one slant at a time, the visual system must derive one estimate from the set of somewhat discrepant signals. In our conceptualization, the weight associated with each slant estimate is a function of its estimated reliability, and the estimated reliability is based in turn on the quality of the information present in the signals (e.g., Landy et al., 1995; Heller & Trahiotis, 1996). Several factors influence signal reliability. For example, consider the effects of increasing viewing distance. As distance increases, there is no effect on the information carried by the perspective signal (assuming broadband texture; Sedgwick, 1986), but the information carried by *HSR* is reduced because a given set of slants maps onto ever smaller ranges of *HSR*. Consequently, nonstereoscopic slant estimates should be weighted more heavily relative to stereoscopic slant estimates as viewing distance increases; experimental evidence confirms this expectation (Buckley & Frisby, 1993; Backus & Banks, 1999).

Some of our experiments examined whether the signals described above are used in estimating slant, and how the weights assigned to the estimates vary across viewing conditions and stimulus properties.

To do these experiments, we built a haploscope that allows independent manipulation of eye position and disparity. We examined the use of the two stereoscopic means of slant estimation described above. (We made nonstereo, perspective information uninformative by using a "back projection" procedure; Banks & Backus,

1998a.) Observers rotated a stereoscopic random-dot plane about a vertical axis until it appeared normal to the line of sight: that is, they adjusted its slant until it was apparently gaze normal. Real and simulated versions were varied from 15• to the left of head-centric straight ahead to 15• to the right. Real version was varied by turning the haploscope arms so that the observer rotated the eyes to the desired version position. Simulated version was varied by altering the disparity field. Thus, an observer might look at a stereo plane with eyes rotated leftward while the disparities presented were as if the eyes were rotated rightward. If the visual system relies on extra-retinal, eye-position signals ($\hat{S}_{HSR,EP}$, slant estimation by *HSR* and eye position) in estimating the slant of a stereoscopic surface, then the observers' settings would be predicted from their actual eye positions; these predictions are represented by the diagonal line in the left panel of Figure 4. If, on the other hand, the system uses the information contained in the disparity field alone ($\hat{S}_{HSR,VSR}$, estimation by *HSR* and *VSR*), the settings would be predicted by the simulated eye positions; these predictions are represented by the three horizontal lines (one for each of three simulated eccentricities) in the left panel of Figure 4.

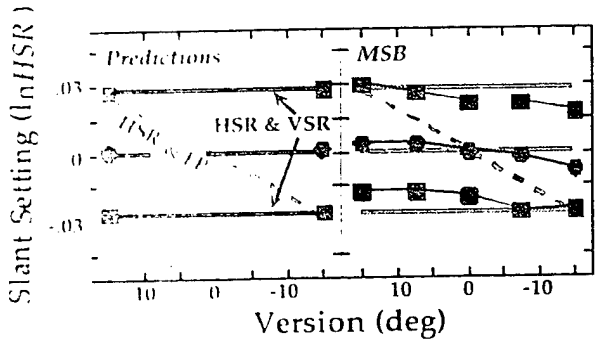

Figure 4. Predictions and results, Backus et al (1999). Natural log of *HSR* settings is plotted as a function of version. Left panel: Predictions. Slant estimation by *HSR* and eye position predicts the diagonal line. Estimation by *HSR and VSR* predicts the three horizontal lines (one for each *VSR*). Right panel. Results from one of 3 observers. Squares, circles, and squares represent results with different *VSR* values.

The results are displayed in the right panel of Figure 4. The data agree quite well with the predictions of $\hat{S}_{HSR,VSR}$. The actual version of the eyes had no clear effect on slant settings which is counter to the predictions of $\hat{S}_{HSR,EP}$. Thus, with large targets, compensation for eccentric viewing is based primarily on the pattern of horizontal and vertical disparities within the images and little on actual eye position. We can summarize these findings by expressing the slant estimates as weighted averages of the signals presented to the visual system: $\hat{S} = w_{H,V}\hat{S}_{HSR,VSR} + w_{H,E}\hat{S}_{HSR,EP}$ where the w's represent the associated weights. We can ignore the nonstereo slant estimator in this experiment (not expressed in equation) because it always specified a slant of 0 and thereby could have no influence in a slant-nulling task. The data in Figure 4 can be fit well by this model if $w_{H,V}$ =.85 and $w_{H,E}$ =.15.

The magnitudes of vertical disparities at a given azimuth are roughly proportional to elevation above the visual plane (*VSR* is, however, constant in the Fick coordinates we use for our equations). Thus, surfaces that subtend a small vertical angle do not create large vertical disparities. We took advantage of this by reducing stimulus height.

The results for one observer are shown in Figure 5. Stimulus width was always 40•, but the height varied from 0–30• (left to right in the figure). When the height was 30•, we again found that slant settings were determined almost exclusively by $\hat{S}_{HSR,VSR}$. However, as stimulus height was reduced, the slant settings became more and more consistent with $\hat{S}_{HSR,EP}$. Finally, with a stimulus height of 0• (horizontal row of dots), slant settings were predicted entirely by $\hat{S}_{HSR,EP}$; thus, as the eyes turned, different patterns of disparity were required for a gaze-normal percept.

These results show clearly that the human visual system employs two means of estimating slant of stereoscopically defined surfaces. The weight given $\hat{S}_{HSR,VSR}$ is high when the stimulus is large and contains measurable vertical disparities. The weight given $\hat{S}_{HSR,EP}$ is high when the stimulus is short and does not contain readily measurable vertical disparities.

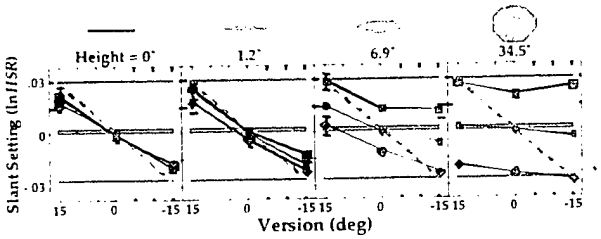

Figure 5. Slant settings for different stimulus heights. Natural log of *HSR* is plotted in each panel as a function of version. Panels from left to right show data when stimulus height varied from 0–35•. Predictions (see Figure 4) are also shown for two means of slant estimation.

In the remainder of this report, we will describe slant estimation by linear combination of information from slant estimators, each weighted in some

statistically reasonable fashion. For example, estimated slant about the vertical axis, can be modeled as:

$$\hat{S} = w_{Stereo}\hat{S}_{Stereo} + w_{Nonstereo}\hat{S}_{Nonstereo}$$

where the weights are positive and add to 1 and

$$\hat{S}_{Stereo} = w_{H,V}\hat{S}_{HSR,VSR} + w_{H,E}\hat{S}_{HSR,EP}$$

The values of the estimators will in general not agree, even in natural viewing, because the signals they use are subject to measurement error. Using linear, weighted combination to derive the final estimate is an example of a weak fusion model (Landy et al, 1995; Clarke & Yuille, 1990). We call it slant estimation theory.

The work described above focused on estimation of surface slant about a vertical axis. Naturally, the visual system must estimate slant about any axis, not just the vertical. One can show that the slant and tilt of a smooth surface can be recovered locally from estimates of the slant component about the vertical axis (tilt = 0•; Stevens, 1983) and the component about the horizontal axis (tilt = 90•) (Backus et al, 1999). Thus, we will investigate slant estimation about the horizontal axis and apply what we learn to estimation about arbitrary axes.

Slant about the horizontal axis produces a vertical gradient of horizontal disparity: so-called horizontal shear disparity. We can quantify horizontal shear disparity as $HSh = 1 + \frac{\delta_H}{\beta_R}$ where the values are defined in Figure 7. Likewise, vertical shear disparity is: $VSh = 1 + \frac{\delta_V}{\beta_R}$. As with *HSR* and *VSR*, we do not claim that *HSh* and *VSh* are measured directly by the visual system as opposed to other quantifications of disparity; rather we use these quantifications because they are convenient mathematically.

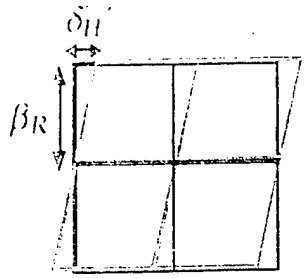

$$HSh = 1 + \frac{\delta_H'}{\beta_R}$$

Figure 6. Definition of *HSh*. Two eye's images are superimposed (black = left eye; gray = right). δ_H is the horizontal offset between two corresponding image points and β_R is the vertical angle between an image point with no disparity to a point with shear disparity.

The eyes can rotate about the lines of sight; these are torsional movements. Cycloversion is torsional eye movements in the same direction and cyclovergence is torsional movements in opposite directions. We define torsional alignment as eye positions for which the eyes' horizontal meridia lie in the same plane. When the eyes are torsionally aligned, slant about the horizontal axis is given to close approximation by:

$$\hat{S} \approx -\tan^{-1}(\frac{1}{\mu}\ln HSh) \qquad (1.3)$$

where μ is horizontal vergence (Banks et al, 1999). When the eyes are not torsionally aligned, the rotation of one eye relative to the other (cyclovergence) alters *HSh* (Howard & Kaneko, 1994), so slant cannot be estimated from Equation (1.3). There are two means by which the visual system could compensate for the change in *HSh* that accompanies cyclovergence.

1) Cyclovergence causes equal changes in *HSh* and *VSh*, so correction could be accomplished by comparing the two disparities (Howard & Kaneko, 1994; Koenderink & van Doorn, 1976). Banks et al (1999) showed in this case that slant is to close approximation:

$$\hat{S} \approx -\tan^{-1}(\frac{1}{\mu}\ln\frac{HSh}{VSh}) \qquad (1.4)$$

We refer to this as slant estimation by *HSh* and *VSh* ($\hat{S}_{HSh,VSh}$).

2) There may exist an extra-retinal signal specifying the eyes' cyclovergence (Nakayama & Balliet, 1977), so correction could occur by using that signal:

$$\hat{S} \approx -\tan^{-1}(\frac{1}{\mu}\ln HSh - \tan\omega) \qquad (1.5)$$

where ω is the eyes' cyclovergence (Banks et al, 1999). We call this slant estimation by *HSh* and eye position ($\hat{S}_{HSh,EP}$).

Usually, greater slant is perceived in stereo-defined surfaces when slant is about the horizontal axis as opposed to the vertical axis (Rogers & Graham, 1983; Mitchison & McKee, 1990; Gillam & Ryan, 1992; Buckley & Frisby, 1993). Because the signals involved are so different for slant estimation about the horizontal axis than for estimation about the vertical axis, there are a variety of possible explanations for this so-called slant anisotropy. Comparing the results from the horizontal axis experiments with our previous work (e.g., Backus et al, 1999) will help delineate the critical differences.

Before discussing our experiments on horizontal-axis slant, we should point out that one can estimate slants with respect to any axis from the size disparities (*HSR* and *VSR*) and shear disparities (*HSh* and *VSh*). We have shown that slant and tilt can be recovered by extension of Equations 1.2 and 1.4 above. Specifically,

$$\sigma = \frac{1}{\mu}[\ln^2 \frac{HSR}{VSR} + \ln^2 \frac{HSh}{VSh}]^{-0.5}$$

$$\tan\tau = \ln\frac{HSR}{VSR} \Big/ \ln\frac{HSh}{VSh}.$$

Similar relationships can be derived for horizontal disparity and sensed eye position.

Now let us return to the discussion of slant estimation with respect to the horizontal axis. Howard and Kaneko (1994) and Kaneko and Howard (1996) observed changes in perceived slant when *HSh* or *VSh* was varied; an increase in *HSh* caused the stimulus to pitch top away and an increase in *VSh* caused it to pitch top forward, as predicted by Equation (1.4). When *HSh* was equal to *VSh*, the stimulus appeared gaze-normal, again as predicted by Equation (1.4). Kaneko and Howard (1996) also looked for an effect of eye position (their Experiment 4), but did not observe one. However, one would not expect to observe an eye-position effect in their experiment for two reasons. First, the stimuli were large random-dot planes, so slant estimation via vertical disparity may have dominated as we observed in the vertical-axis experiments (Figure 5). Second, to stimulate cyclovergence, they presented a 5-sec, cyclorotated pattern; cyclovergence is slow, so this stimulus may not have created large enough movements to observe a perceptual effect. They did not measure cyclovergence, so one cannot assess this possibility.

At ARVO in 1999, we presented data on slant estimation about the horizontal axis (Banks et al, 1999). This work is currently being written up as two papers for *Vision Research*. One paper (Banks et al, 2000) contains the theoretical work and stereo experiments and the other (Hooge et al, 2000) contains our experiments on measurements of cyclovergence.

The goal in the stereo experiments was to vary cyclovergence and *VSh* independently to determine whether the two estimation methods exist and, if so, how their outputs are combined. The experimental procedure is depicted in Figure 7. We induced cyclovergence with a conditioning stimulus composed of horizontal lines; the lines were rotated in opposite directions in the two eyes. We measured cyclovergence response using a nonius technique. The nonius figure (upper right panel) was flashed and the observer judged whether the lines were subjectively parallel. We validated the nonius technique by using 3-D search coils in van den Berg's lab in Rotterdam. Observers performed the nonius task while eye position was measured. Nonius and objective measures agreed closely (Hooge et al, 2000).

We conducted three stereo experiments. In the first, the stimulus used to measure perceived slant was a large random-dot plane; the dots were back-projected to render nonstereo slant signals uninformative. Different amounts of *VSh* were added to the stimulus. The plane was flashed and the observer adjusted *HSh* until the plane appeared gaze normal (lower right panel). The procedure cycled between the conditioning stimulus (2 sec), nonius figure (100 msec), conditioning stimulus (2 sec), test stimulus (100 msec), and so forth until the observer was satisfied with both settings. By using this procedure, we knew the eyes' cyclovergence.

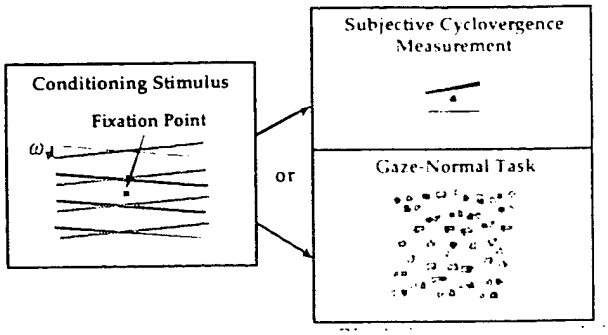

Figure 7. Experimental procedure. Black lines represent left eye's image and gray lines right eye's image. Conditioning stimulus (left) is presented to induce cyclovergence. Nonius technique (upper right) is used to measure cyclovergence; observers adjust orientation of upper line until subjectively parallel to lower. Gaze-normal task (lower right) is used to measure slant percepts. Observers adjust *HSh* until random-dot plane appears gaze normal.

Predictions for the gaze-normal task are shown in the left panel of Figure 8. Cyclovergence response is plotted on the abscissa and *HSh* (at the screen) on the ordinate. (For convenience, *HSh* is expressed in equivalent degrees of cyclorotation.) If no compensation occurred for changes in cyclovergence, gaze-normal settings would be predicted by Equation (1.3); the data would lie on the diagonal line. If complete compensation occurred based on *VSh* (Equation 1.4), the data would lie on the five horizontal lines. If complete compensation occurred based on eye-position signals (Equation 1.5), data would lie on the horizontal line at $HSh = 0$.

Data from one of the three observers are shown in the right panel of Figure 8. The data are consistent with slant estimation by *HSh* and *VSh* except when *VSh* was opposite in sign from cyclovergence (upper left and lower right parts of the figure). We cannot determine whether those deviations reflect the contribution of eye-position signals or a failure to compensate because *VSh* was so large in those cases.

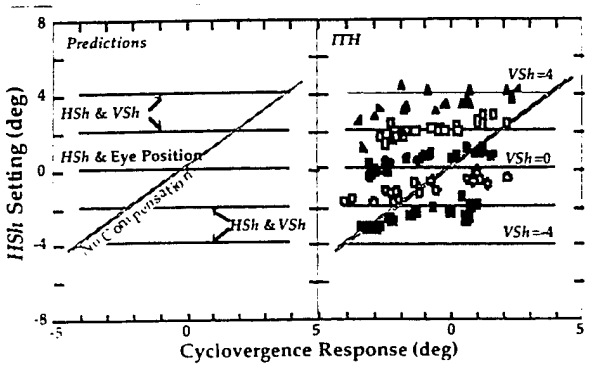

Figure 8. Predictions and results. *HSh* at the screen (expressed in deg) is plotted as a function of the cyclovergence response. Left panel: Predicted *HSh* settings for the three hypotheses. Right panel: Individual settings for observer ITH. From top to bottom, *VSh* (in deg) was 4, 2, 0, –2 and -4 deg. Different symbols represent the different *VSh*'s.

Experiments 2 and 3 were designed to determine which is the better account. In Experiment 2, we reduced the diameter of the random-dot plane to 5 deg; this made *VSh* difficult to measure. In Experiment 3, the stimulus was a single smooth vertical line; this makes *VSh* impossible to measure because there are no vertically separated features. In both cases, we found a complete failure to compensate for the eyes' cyclovergence. In other words, when we induced cyclovergence changes, the observer saw different slants in the stimulus. It appears then that compensation for cyclovergence is mediated only by use of vertical disparities. We found no evidence for use of an extra-retinal signal.

During the past year, we completed two other experiments and manuscripts concerning surface perception. One involved an analysis of binocular slant contrast (van Ee et al, 1999) and the other involved use of haptic feedback to adjust the weights given to different slant estimators (Ernst et al, 2000). We also completed data collection and analysis on an experiment on real-world slant perception. The manuscript is in draft form (James et al, 2000).

We begin by describing our analysis of slant contrast. There are several stereoscopic phenomena in which the perceived slant or curvature of a surface patch is not what one would predict from the disparities. The presence of these illusions has been taken as evidence that visual system does not interpret retinal disparity accurately and thus does not derive from stereopsis an accurate 3D representation of the scene (e.g., Poggio, et al, 1988). Furthermore, explanations for the illusions have included special assumptions about the form of disparity-encoding mechanisms (Rogers & Graham, 1983), internal biases (Gogel, 1956), reference frames (van Ee & Erkelens, 1996), and other assumptions. We believe that slant estimation theory can account for many of these illusions; that is, they might be understood by analyzing the available signals and their statistical reliabilities without assumptions about underlying mechanisms. We propose analyzing some well known stereoscopic illusions and conducting experiments to determine if the analyses are valid.

One such illusion is the slant-contrast effect illustrated in Figure 9. When cross-fused, the cross-hatched planes create the *HSR* associated with a plane rotated about a vertical axis (left side far). The strip of dots is identical in the two eyes, so it creates the *HSR* associated with a frontal plane. The dot strip, however, appears rotated in the direction opposite from the specified slant of the cross-hatched planes. The illusory slant is the slant-contrast effect (van Ee et al, 1999).

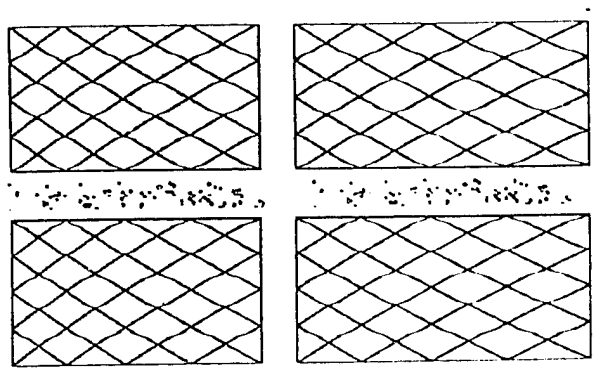

Figure 9. The slant-contrast effect. Cross fuse. The images of the strip of dots are identical in the two eyes, but the strip appears rotated left side near.

Werner (1937, 1938) first described the effect and pointed out that the perceived slant of the surrounding stimulus (the *inducer*) was less than the slant specified by its disparity gradient and that the perceived slant of the internal stimulus (the *test strip*) was opposite to the disparity-specified slant of the inducer. Since then slant contrast has been reported for a wide variety of stimuli (Ogle, 1946; Harker, 1962; Pastore, 1964; Pastore & Terwilliger, 1966; Nelson, 1977; Graham & Rogers, 1982; Stevens & Brookes, 1988; Fahle & Westheimer, 1988; Brookes & Stevens, 1989; Howard et al, 1993; van Ee, 1995; van Ee & Erkelens, 1996a; Pierce et al, 1998).

There are many explanations for slant contrast (Howard & Rogers, 1995; van Ee et al, 1999); they involve special assumptions that, as we will show, may not be necessary.

We adopted slant estimation theory for the analysis of slant contrast (van Ee et al, 1999). Recall that this

theory incorporates all the signals presented in the stimulus and models the resulting slant percepts from linear combination of slant estimators weighted by their assumed statistical reliabilities. To see how it explains slant contrast, consider first the two parts of the stimulus in isolation. The physical slants of the inducer and test strip are S_i and S_t. The perceived slants of the isolated inducer and isolated test strip are given by:

$$\hat{S}_{i,alone} = w_{id}\hat{S}_{id} + w_{ip}\hat{S}_{ip} \qquad (1.6)$$

$$\hat{S}_{t,alone} = w_{td}\hat{S}_{td} + w_{tp}\hat{S}_{tp} \qquad (1.7)$$

Subscripts i and t refer to the inducer and test strip, and d and p to stereo and nonstereo (*d*isparity and *p*erspective). The weights are positive and add to 1. The stereo estimates ($\hat{S}_{id}$ and $\hat{S}_{td}$) are based on the gradients of horizontal disparity created by the test strip and inducer (plus other signals correcting for distance and azimuth). Similarly, the nonstereo estimates are based on nonstereo perspective cues created by the strip and inducer.

The process of estimating the inducer and test strip slants from the signals they create is depicted in Figure 10. For the test strip in isolation, the stereo- and nonstereo-specified slants are both zero, so the slant estimators on average specify slants of zero and the final slant estimate is on average zero. For the inducer in isolation, the stereo-specified slant and nonstereo slant differ: the former is varied and the latter is always zero. The final slant estimate is a compromise between the stereo- and nonstereo-specified slants.

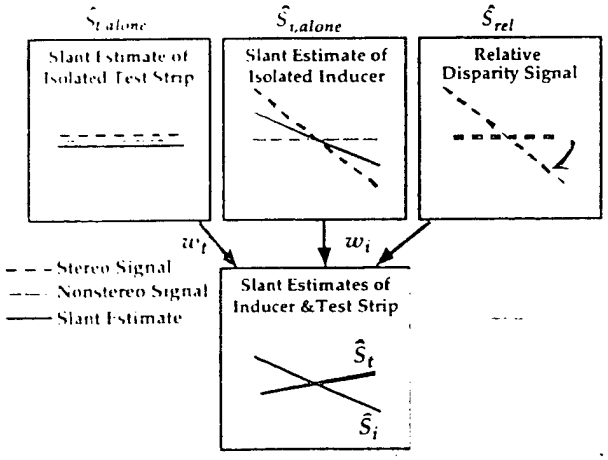

Figure 10. Slant estimation with the slant-contrast stimulus. The inducer's nonstereo-specified slant is inconsistent with its stereo-specified slant. The upper panels, from left to right, depict slant estimates from, respectively, test-strip signals alone, inducer signals alone, and signals between the two. The lower panel depicts the final slant estimates for the strip and inducer.

We also need to consider signals created jointly by the two parts of the stimulus. S_{rel} ("relative slant") is the difference between the slants of the two surfaces, specified by disparity. S_{rel} is based on the disparity gradient between the two surfaces (plus other signals needed to correct for distance and azimuth).

If all three stereo estimators ($\hat{S}_{td}$, $\hat{S}_{id}$, and $\hat{S}_{rel}$) are unbiased, it will on average be the case that:

$$\hat{S}_{td} = \hat{S}_{id} + \hat{S}_{rel}. \qquad (1.8)$$

In the natural environment, signals created by two surfaces in isolation (equations 1.6 & 1.7) and by the signal created between the surfaces (equation 1.8) are on average consistent with one another. In the slant-contrast stimulus, they are not. To see how, first consider the signals from the surfaces in isolation (equations 1.6 & 1.7): the estimate for the inducer in isolation ($\hat{S}_{i,alone}$) will be different from both its stereo-based and nonstereo-based estimates: $\hat{S}_{i,alone} \neq \hat{S}_{id} \neq \hat{S}_{ip}$. Thus, the slant difference specified by the isolated signals is not the same as that specified by the joint signal. Slant estimation theory states that the visual system reconciles the disagreement by combining information from the available signals and weighting each information source according to its estimated reliability. For the test strip:

$$\hat{S}_t = w_t\hat{S}_{t,alone} + w_t(\hat{S}_{i,alone} + \hat{S}_{rel}). \qquad (1.9)$$

The first term is based on signals from the test strip alone and the second term on signals created by the inducer alone and the relative disparity gradient between the inducer and test strip.

The inducer's slant estimate is in principle subject to the same constraints–the test strip inducing slant in the inducer–but, by its construction, the slant-contrast stimulus specifies the inducer's slant much more reliably than the strip's slant (van Ee et al, 1999). Thus, for the stimulus in Figure 9, we can ignore the strip's effect on the inducer.

The relative reliabilities of the slant estimates derived from the first and second terms in Equation (1.9) determine their weights. The second estimator will be no more reliable than its least reliable term; if $\hat{S}_{i,alone}$ and $\hat{S}_{rel}$ are uncorrelated, their reciprocal reliabilities (variances) will add.

We can now predict the apparent slant of the test strip. From equations 1.6–1.9, $w_{id} = 1 - w_{ip}$ (by definition), and the assumption of unbiased estimators:

$$\hat{S}_t = w_t S_{t,alone} + w_i[S_{id} - w_{ip}(s_{id} - S_{ip})]. \qquad (1.10)$$

If the indirect estimate of test strip slant is much more reliable than the direct measure, then $w_t \approx 0$.

Furthermore, in the slant-contrast stimulus, $S_{id} = S_{ip} = 0$, so

$$\hat{S}_t = -w_{ip} S_{id} . \qquad (1.11)$$

The predicted perceived slant of the test strip is thus opposite to the inducer's stereo-specified slant (S_{id}) and is proportional to the weight of the inducer's nonstereo-specified slant (w_{ip}). We showed experimentally that this equation predicts slant contrast effects accurately (van Ee et al, 1999).

According to slant estimation theory, slant contrast is a byproduct of the visual system's attempt to reconcile the inconsistency between the stereo- and nonstereo-based signals produced by the inducer. It follows that slant contrast would not be observed if the inconsistency were eliminated by making the inducer's stereo and nonstereo signals consistent: in Equation 1.10, the term weighted by w_{ip} becomes zero. We confirmed this prediction once all inducer signals, including those arising from the surface of the CRT, were consistent (van Ee, et al, 1999). Notice that the prevailing theory of slant contrast (Rogers & Graham, 1983; van Ee & Erkelens, 1996; Howard & Rogers, 1995) would predict no effect of altering the inducer's nonstereo-specified slant.

During the past year, we also examined the question of how the visual system determines how much weight to give to one means of slant estimation as opposed to another. Specifically, we examined how the weights given disparity and texture cues are determined. There are at least three possibilities. 1) Fixed weights: the weights are fixed for a given situation and individual and not subject to change through feedback. 2) Comparison with other estimators: the weights are learned over time by comparing a given estimator's output with those of other estimators and with feedback from motor behavior. 3) On-line determination: the weights are determined directly from measuring the statistics of estimator output; for example, if the output of one estimator fluctuates less over time than that of another estimator, the weight of the former should be increased relative to the weight of the latter.

The second and third possibilities are not mutually exclusive: both means of weight determination could co-exist in a given estimator.

We conducted an experiment with Marc Ernst, a Physics graduate student, that was designed to examine the second of the above hypotheses. Specifically, we asked whether visuomotor feedback could affect the weights given to stereo and nonstereo slant estimators.

The experimental setup is schematized in Figure 11. The visual display was viewed in a mirror placed above the hand. The index finger and thumb of the right hand were placed in separate haptic feedback devices (depicted beneath the mirror). The Phantom feedback devices provided force to the finger and thumb and thereby simulated a virtual surface.

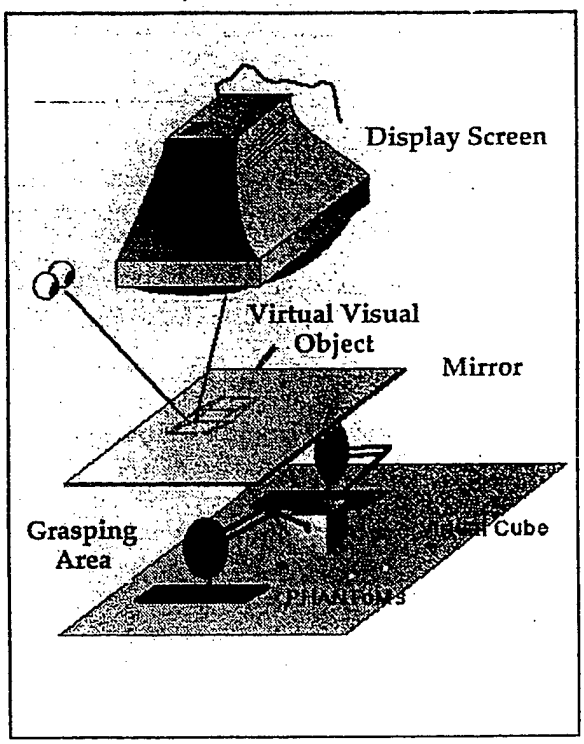

Figure 11. The experimental setup for the haptic feedback experiment. The visual stimulus is presented in the display screen above and viewed in the mirror placed above the hand. The index finger and thumb of the right hand are placed in Phantom haptic feedback devices. The observer touches and grasps virtual objects in the workspace. Haptic feedback creates the sensation of touching a real object or surface.

The experiment had three phases which are depicted in Figure 12: 1) pre-adaptation, 2) adaptation, and 3) post-adaptation. The pre- and post-adaptation phases were purely visual tasks. The visual stimulus in those phases was a plane slanted about a vertical axis. Its slant was specified in two ways: 1) Nonstereo signals consisting of the texture gradient and outline shape and 2) stereo signals consisting of geometrically correct disparity gradients. The nonstereo- and stereo-specified slants differed by ±30, ±20, or ±10 deg. Observers adjusted the slant of the perceived surface until it appeared gaze normal; the adjustment affected the nonstereo- and stereo-specified slants equally thereby holding the difference between them constant. Although no feedback was given during the pre- and post-adaptation phases, observers had no difficulty

performing this task. They were also unaware of the conflict between the slant signals.

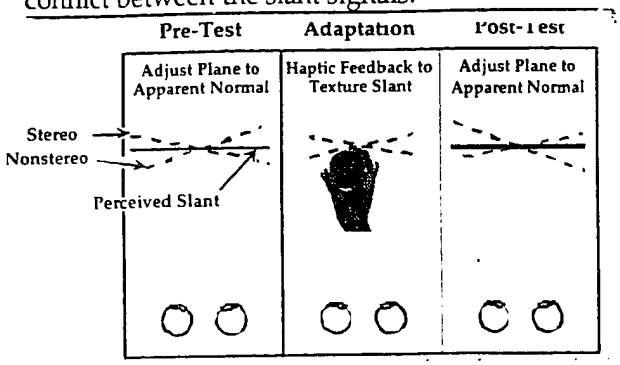

Figure 12. Experimental design for haptic feedback experiment. The three lines in the left and right panels represent the stereo-and nonstereo-specified slants as well as the slant percept. See text for details.

During the adaptation phase, the Phantom provided haptic feedback. Observers pushed a small visible cube with the index finger to targets on a visible slanted plane. Haptic feedback was given according to the nonstereo-specified and not the stereo-specified slant. The difference between the nonstereo and stereo slants was random during adaptation, so haptic feedback was only correlated with the nonstereo-specified slant. The adaptation phase lasted 30–45 minutes. Observers were questioned after the experiment: they were not aware that the haptic feedback was unusual in any way.

The results are shown in Figure 13 which plots the slant settings from the pre- and post-adaptation phases. The nonstereo-specified slant of the surface when it appeared gaze normal is plotted as a function of the difference between the nonstereo- and stereo-specified slants. By performing linear regression on these data, we can determine the weights given nonstereo- and stereo-specified slants. The average stereo weight was 0.70 during pre-adaptation and 0.55 during post-adaptation. Although this is a small change, all eight observers exhibited the decrease, so the effect is highly significant statistically. This suggests that haptic feedback during the adaptation phase produced a downweighting of the stereo slant estimator. There have been numerous demonstrations that changing the relationship between vision and haptic feedback can affect motor behavior (reviewed by Welch, 1986 and Harris, 1980), but we believe this is the first demonstration that haptic feedback affects judgments in a purely visual task.

We also tested some alternative explanations for these data. Perhaps the decrease in stereo weight resulted from increased experience with the visual displays and not from the low correlation between haptic feedback and nonstereo-specified slant during the adaptation phase. We can rule this out because we observed no decrease in stereo weight when nonstereo- and stereo-specified slants were identical during the adaptation phase. Perhaps the visual experience of seeing a cube move along a nonstereo-defined surface and not along a stereo-defined surface causes a change in weight. To test this possibility, we recorded the sequence of visual images presented during the adaptation phase of each observer in the main experiment and showed those sequences to control subjects. Although they experienced the same sequence of images, they did not exhibit a change in stereo weight.

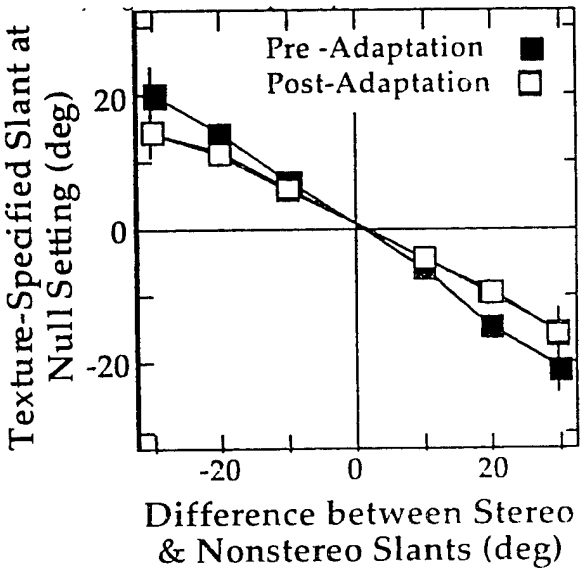

Figure 13. Results from haptic feedback experiment. Slant settings are shown for the pre- and post-adaptation phrases. The nonstereo-specified slant of the visual stimulus, when it appeared gaze normal, is plotted as a function of the difference between the nonstereo- and stereo-specified slants. The data points are averages from 8 observers' settings.

We have shown that haptic feedback affects surface perception in a purely visual task. Specifically, giving haptic feedback consistent with one slant estimator has the effect of increasing the weight assigned to that estimator. This observation is consistent with the view that calibration of spatial vision occurs, at least in part, as a consequence of motor interaction with the environment.

This work appeared recently in *Nature Neuroscience* (Ernst et al, 2000). It has received quite a bit of attention in the media as well. It was written up in the southern German newspaper: *Süddeutsche Zeitung*: (the article was entitled "Der Mensch sieht auch mit den Händen" which means that people see with their hands). It is posted on a news bulletin on the web: http://www.mpg.de/pri00/pri6_00.html and Dr. Ernst was interviewed about this study on a local radio

station: "Hessischer Rundfunk". In addition, Dr. Ernst won the Attempto Preis for this work. This prize is an annual award given to the best work in neuroscience in the southern German area.

Very recently, we have completed an investigation into the perception of slant with real-world objects. In collaboration with Fiona James and Tutis Vilis of the University of Western Ontario, we examined how people take eye position into account when asked to judge the slant of a surface in world coordinates. To judge slant relative to the world, the nervous system must measure surface slant relative to the line of sight (oculocentric slant), eye position relative to the head, and head position relative to the world coordinates. We showed two things: 1) people are quite good at judging object slant in world coordinates and 2) their errors are the outcome of errors in all three measurements. This work was reported at ARVO this year (James et al, 2000) and is currently being written up for publication in *Vision Research*.

2. Heading Perception

We have also continued our research on the perception of self-motion. During the past two years, five publications appeared from this project: Crowell et al (1998), Ehrlich et al (1998), Freeman and Banks (1998), Freeman (1999), and Freeman et al (2000). In addition, we have completed the theoretical analysis and preliminary experiments on another project which was reported this year at ARVO (Sibigtroth et al, 2000). We also completed construction of our 3-axis rotating chair in which we are conducting visual-vestibular research that is relevant to spatial disorientation in aviation.

As in the previous section, we will first review the background material for this research project before moving onto the particular experiments and analyses that were completed. Much of this background section also appeared in last year's progress report, so if you read it previously, you may want to skip ahead to page 11.

As a person moves through the natural environment, images move across the retina, the eyes move relative to the head, the head turns relative to the body, and the body translates and rotates through space. Despite this complex of various motions, the nervous system produces a coherent percept of the person's motion relative to environmental landmarks. From this percept, the human observer is able to move toward targets, avoid obstacles, and guide complicated perceptual-motor behavior. We have been examining how the nervous system accomplishes this. Our work has examined the analysis of visual signals, eye-velocity signals, head-velocity signals, and more. We begin this part of the report by describing work we did on how the visual takes the motion of the retinal image and the motion of the eye in the head into account when judging the velocity of an object.

If the body and head are stationary, the head-centric velocity of an object (H) is the sum of retino-centric velocity (R) and eye velocity (P). Perceived head-centric velocity will be affected by errors in the visual system's measurements of R or P. We assume that the perceived velocity ($\hat{H}$) is the sum of estimated retino-centric velocity ($\hat{R}$) and estimated eye velocity ($\hat{P}$). Assuming that $\hat{P}$ is linearly related to eye speed, we have: $\hat{P} = eP$, where e is the extra-retinal gain factor relating actual to estimated eye speed. $\hat{R}$ is the estimated retinal image velocity, so making the linear assumption: $\hat{R} = r(\Omega)R$, where r is the retinal gain relating actual to estimated retino-centric speed which is affected by a variety of stimulus properties (Ω) including spatial frequency, contrast, and size. It is surprising that variations in retinal gain have not been incorporated in most previous models of head-centric velocity perception. We assume a single value for r for each value of Ω. Our model of perceived head-centric velocity is, therefore:

$$\hat{H} = r(\Omega)H + P[e - r(\Omega)]. \qquad (2.1)$$

r and e are unknown properties of the visual system; the other variables are physical quantities. The parameters of this model were measured in speed-matching experiments with gratings of different spatial frequencies (Freeman & Banks, 1998).

When an observer makes a pursuit eye movement, while being presented a target stationary with respect to the head, the Filehne illusion occurs: The target appears to move opposite to the eye movement. The conventional explanation for the illusion is that the gain of the extra-retinal, eye-velocity signal (e) is less than 1, so it under-estimates actual eye speed during pursuit movements (Mack, & Herman, 1973, 1978; Yasui, & Young, 1975); the implicit assumption is that the retinal gain (r) is 1. We examined this classic illusion in the context of our model.

When the perceived speeds of two stimuli are equal, $\hat{H}_T = \hat{H}_S$, where the subscripts refer to the test and standard stimuli. With this equality, Equation (2.1) can be rewritten:

$$\frac{r(f_T)}{r(f_S)} = \frac{H_S}{H_T} \qquad (2.2)$$

where $r(f_S)$ and $r(f_T)$ are the retinal gains for the standard spatial frequency and the test spatial

frequency, respectively. Equation (2.2) suggests that the magnitude of the Filehne illusion ought to depend on the spatial frequency of the target. The Filehne illusion is usually measured by setting the target's speed such that it appears stationary with respect to the head. In this case, $H_S = 0$, so Equation (2.2) becomes:

$$H_T = P[1 - \frac{\tilde{e}}{\tilde{r}(f_T)}] \qquad (2.3)$$

where $e = \frac{r(f_T)}{r(f_S)}$ and $\tilde{e} = \frac{e}{r(f_S)}$. For a given pursuit speed, P is constant and we assume that $\tilde{e}$ is constant as well. When $\tilde{r}(f_T) > \tilde{e}$, equation (2.3) predicts that H_T must have the same sign as P for the target to appear stationary; this prediction is consistent with the classical literature. However, when $\tilde{r}(f_T) < \tilde{e}$, which could occur at low spatial frequencies where retinal gain is low, the equation predicts that H_T must be opposite in sign from P for the target to appear stationary. This prediction is opposite to the conventional Filehne illusion. There is one report of a reversed Filehne illusion (Wertheim, 1987). We were able to confirm the predictions of Equation (2.3) quite accurately across an 8-fold range of spatial frequencies. Specifically, we observed the reverse Filehne illusion at the spatial frequencies predicted by the model.

We also examined the Aubert-Fleischl illusion in which a moving object appears to move more slowly when it is tracked with a pursuit eye movement than when it is not tracked. As with the Filehne, the Aubert-Fleischl illusion has been assumed to result from an extra-retinal gain (e) less than 1; the implicit assumption again is that the retinal gain (r) is 1. Again the model predicts that the Aubert-Fleischl illusion should reverse at low spatial frequencies and we were able to confirm this experimentally. Figure 14 summarizes the results of this experiment (details in the caption).

Our model and data make clear that the perception of head centric speed is affected by errors in estimating speed of eye movement and by errors in estimating speed of retinal-image motion (Freeman & Banks, 1998). The latter finding is particularly important for understanding effects of lowpass filtering and contrast reduction that occur with visual aids such as night-vision goggles.

We also applied what we learned in the above study to the problem of estimating heading during gaze rotations. In particular, we examined the timing and gain of extra-retinal, eye-velocity signals while people perform a self-motion estimation task (Freeman, 1999; Freeman, Banks, & Crowell, 2000). Here we describe that work very briefly.

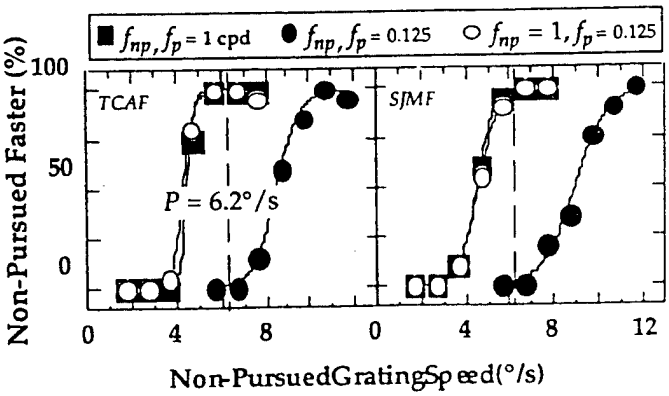

Figure 14. Aubert-Fleischl illusion as a function of spatial frequency. Observers reported whether a pursued or non-pursued grating moved faster relative to the head. The panels plot the percentage of responses that the non-pursued grating appeared faster as a function of the non-pursued grating's speed. Eye pursuit speed was 6.2deg/s (vertical dashed line). Filled squares represent data when the frequency of pursued and non-pursued gratings was 1 cpd. Filled circles represent data when the gratings' frequency was 0.125 cpd. Open circles represent the data when the frequencies of pursued and non-pursued gratings were 0.125 and 1 cpd, respectively.

To judge stimulus motion relative to the head, the visual system must correct for any eye movement the occurs by using an extra-retinal, eye-velocity signal. Such correction is important in a variety of motion estimation tasks including judgements of object motion relative to the head and judgements of self-motion direction from optic flow. Speed and timing errors were investigated using sinusoidal pursuit eye movements. We described a new illusion—the slalom illusion—in which the perceived direction of self-motion oscillates left and right when the eyes moves sinusoidally. The linear model of Freeman and Banks (1998) was used to determine the gain ratio and phase difference of extra-retinal and retinal signals accompanying the Filehne illusion and slalom illusion. The speed mismatch and timing differences were measured in the Filehne and self-motion situations using a motion-nulling procedure. Timing errors were very small for the Filehne and slalom illusions. However, the ratios of retinal gain and extra-retinal gain were consistently less than one, so both illusions are the consequence of a mismatch between estimates of retinal and extra-retinal speed.

The results are quite relevant to aviation because this work shows that errors in self-motion estimation

can occur during pursuit eye movements and that those errors are dependent on the type of visual stimulus presented to the pilot. The linear model allows us to make reasonably general statements about the relationship between stimulus parameters and misperceptions of self-motion during eye movements.

We also continued our work on the use of various signals to estimate the direction of self-motion. The problem we examined in the *rotation problem*, so we begin with a description of that problem, followed by a brief literature review, and then by a description of our work during the grant period.

As we move through the environment, the retinal image of that environment changes in predictable ways. For example, if we move in a straight line our self-motion produces a radial pattern of motion in the retinal image, like that in Figure 15A. The center or focus of the radial expansion (marked by a '+' in Figure 15) corresponds to our direction of motion (Gibson, et al, 1955). Re-creating this pattern of retinal-image motion by viewing a film or computer display depicting our forward motion can cause a compelling sensation that we are in fact moving forward (Howard, 1982), and under a variety of conditions we can accurately estimate where we are going in the simulated scene (Warren et al, 1988; Royden et al, 1992).

When we smoothly shift gaze direction by turning the eye or head (e.g. to look at a moving object or a stationary object to the side) while still moving in a straight line, the pattern of retinal-image motion is more complex (Figure 15B). We can re-create this type of retinal motion pattern by having observers hold the eyes still while viewing a display that simulates both their forward motion and an eye movement. In this case, observers report that they are moving along a curved trajectory (as though turning a car while looking forward through the windshield) rather than along the depicted linear path. When they are asked to adjust the position of a marker in front of them until it appears to sit upon their future path, their responses are strongly biased in the direction of the perceived path curvature (Royden et al, 1992, 1994; Banks et al, 1996; van den Berg, 1996). On the other hand, self-motion judgments are quite accurate when the identical pattern of retinal image motion is created by having observers view a display like that in Figure 15A while turning the eye to pursue a target that moves across it (Royden et al, 1992, 1994; Banks et al, 1996; van den Berg, 1996). Observers typically report that they appear to be moving on a straight rather than a curved path (Royden, 1994). In this case, the observer's visual system has extra-retinal information about the eye movement, probably consisting mainly of an efference copy of the motor command to turn the eye (Howard, 1982). The visual system uses this information to compensate for the effects of the eye movement on the retinal motion pattern; previous research using self-motion judgments indicates that this compensation is nearly complete.

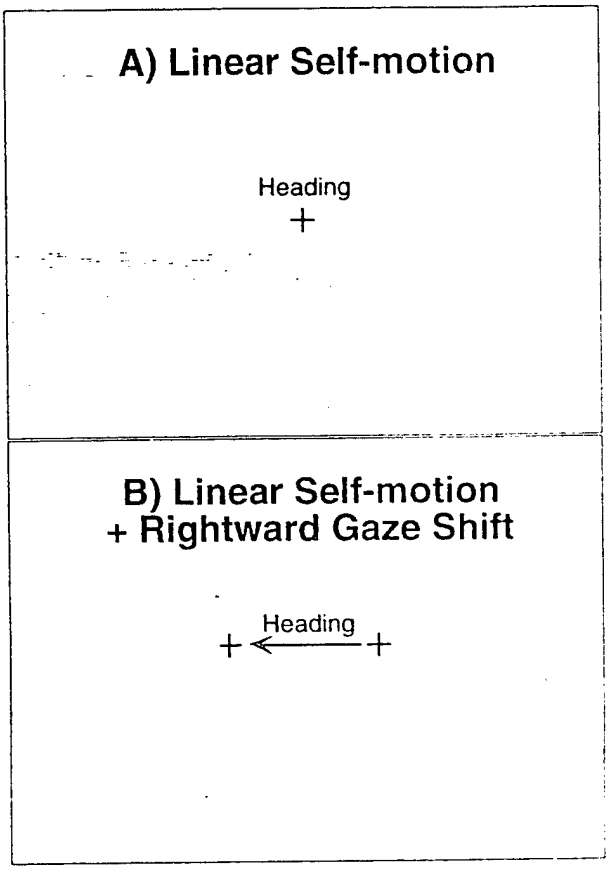

Figure 15. Retinal flow fields for two viewing situations. A) Forward translation without a gaze rotation. Observer is fixating in constant direction and heading toward the cross. B) Forward translation while making a gaze rotation. Observer is making a rightward eye movement.

During the grant period, we examined the contribution of depth information to estimating the direction of self motion. This work appeared in a paper by Ehrlich and colleagues in *Vision Research* in 1998. Here we describe that work briefly.

When presented with random-dot displays with little depth information, observers cannot determine their direction of self-motion accurately in the presence of rotational flow without appropriate extra-retinal information (Royden, et al 1994). On theoretical grounds, one might expect improved performance when depth information is added to the display (van den Berg & Brenner, 1994a). We examined this

possibility by having observers indicate perceived self-motion paths when the amount of depth information was varied. When stereoscopic cues and a variety of monocular depth cues were added, observers still misperceived the depicted self-motion when the rotational flow in the display was not accompanied by an appropriate extra-retinal, eye-velocity signal. Specifically, they perceived curved self-motion paths with the curvature in the direction of the simulated eye rotation. The distance to the response marker was crucial to the objective measurement of this misperception. When the marker distance was small, the observers' settings were reasonably accurate despite the misperception of the depicted self-motion. When the marker distance was large, the settings exhibited the errors reported previously by Royden et al (1994). The path judgment errors observers make during simulated gaze rotations appear to be the result of misattributing path-independent rotation to self-motion along a circular path with path-dependent rotation. An analysis of the information an observer could use to avoid such errors reveals that the addition of depth information is of little use.

During the grant period, we completed a project on how the visual compensates for head rotations in estimating self-motion; the manuscript appeared in *Nature Neuroscience* (Crowell, et al, 1998) and was also reviewed favorably in *Science News*.

In our previous work, we examined perception of self-motion during gaze rotations caused by a smooth pursuit eye movement. Of course, gaze rotations in everyday perception, including aviation, occur due to rotations of the eye, head, and body (and various combinations of those). We examined human ability to estimate self-motion paths during gaze rotations caused by head and body rotations. Figure 16 depicts the three sorts of self-motion conditions presented in this experiment. In each case, the depicted self-motion path was forward over a ground plane with a path-independent rotation (about a vertical axis). The simulated rotation condition is the same as used previously by Royden et al (1994) and Banks et al (1996). In the head-rotation condition, observers made an active head rotation (about a vertical axis). Observers fixated a moving point such that no rotation of the eye relative to the head was required to maintain gaze direction on the moving fixation point. Observers were trained to make smooth head movements of the correct velocity; during the experiment itself, the head movements were measured and trials were thrown out when the movement did not meet pre-established velocity and position criteria. In the body-rotation condition, observers were rotated passively in a vestibular chair; again they fixated a moving point such that no rotation of the eye relative to the head occurred and such that no rotation of the head relative to the body occurred. (This experimental condition was conducted in Richard Andersen's laboratory at Caltech). The retinal images were identical across the three gaze-rotation conditions, so differences in performance must manifest differences in the usage of different extra-retinal signals. In all conditions, observers made judgments of the perceived self-motion path.

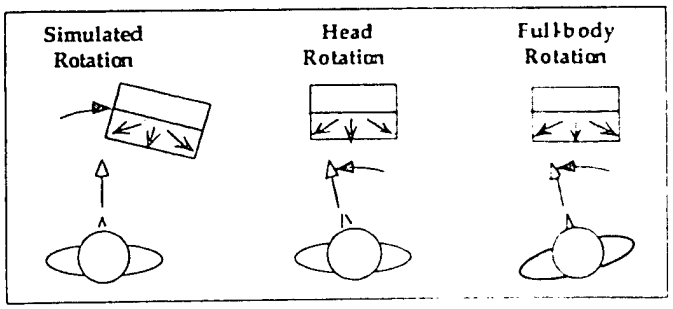

Figure 16. Gaze rotation conditions: Simulated gaze rotation (no rotation of eye, head, or body), head rotation (rotation of head relative to the body), and body rotation (rotation of the body relative to the world). The retinal images are identical across the three conditions.

The results from one of six observers are displayed in Figure 17. The unfilled circles in the left and right panels represent the path judgments from the simulated gaze rotation condition. As we have observed before, observers perceive curved paths in this condition and thus make systematic path judgment errors. The filled squares in the left panel represent the path judgments from the head rotation condition; the errors were small, much as they were during real eye rotations (Royden et al, 1994). This finding suggests that some signal issued during active head rotations is used in estimating self-motion paths. When the head rotates actively, three signals are created: efferent signals to the neck muscles, proprioceptive signals among the neck muscles, and signals from the semi-circular canals. The body rotation condition was run to help determine which of those signals is used: In a full-body rotation, efferent and proprioceptive signals from the neck muscles are not created, so only canal signals are. The crosses in the right panel are the data from the body rotation condition. As you can see, large errors were observed; indeed, the data are essentially

identical to those in the simulated gaze rotation condition (unfilled circles). This finding suggests that the presence of canal signals do not reduce the bias observed during simulated rotations. (A control condition showed that canal signals were suprathreshold.) In other words, canal signals do not play the same role as extra-retinal signals from rotations of the eye relative to the head and of the head relative to the body. This is an extremely important finding that clearly has relevance to our understanding of some illusions experienced by pilots of high-performance aircraft. One of the main themes in the research proposed for the next grant period is to continue this line of investigation into the use of the variety of extra-retinal signals (particularly when they conflict as occurs in aviation) that are issued during self-motion.

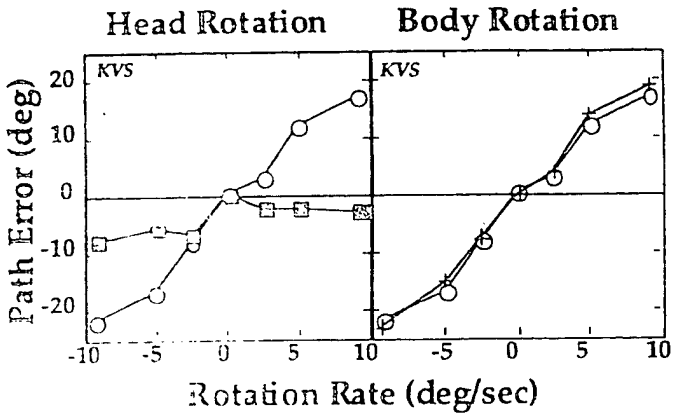

Figure 17 Path judgment errors during simulated gaze rotations, head rotations, and body rotations. Path errors are plotted as a function of gaze rotation rate. Unfilled circles: simulated gaze rotations. Filled squares: active head rotations. Crosses: full-body rotations.

During the past year, we also began to investigate how stimulation of the otoliths (the parts of the vestibular apparatus that signal linear acceleration) affects the perception of heading. Such investigations are clearly relevant to understanding visual-vestibular illusions that occur in aviation such as the pitch-up (somatogravic) illusion and the bank illusion (which can lead to the death spiral).

We presented subjects optic flow displays simulating forward translation and a gaze rotation (see Figure 15B). Normally, observers say they perceive curvilinear self-motion with such displays. We found, however, if we rolled observers to simulate correct or incorrect centrifugal force, we could strongly bias their percepts of self-motion path. This is preliminary work, but its success shows that we can examine the use of otolith stimulation in self-motion perception from optic flow. This work has not been presented at a scientific meeting yet.

We also began an investigation of how perspective transformations affect humans' ability to estimate self-motion. The first set of experiments was presented at ARVO this year (Sibigtroth et al, 2000). The optic flow field created by self-motion through a rigid environment is an important cue to direction of self motion, but it's not the only visual cue. Consider, for example, the case when you walk by a rectilinear building. If you pass to the left side of a corner of a building, you will see more of the wall on the corner's left side over time. If you pass to the right of the corner, you will see more of the wall on the corner's right side over time. The visual system can take advantage of this perspective information (assuming that the corner is indeed a right angle and that the walls are indeed constructed of rectangles) to estimate the heading. Jeremy Beer at Brooks AFB had a similar insight a few years ago and showed the people are sensitive to this information. During the grant period, we worked through the mathematics and showed how this perspective transformation information could be used to determine the direction of self-motion. We then conducted some preliminary experiments (presented at ARVO) that showed that human observers do indeed use this information to estimate heading. This summer we are conducting the final set of experiments before writing it up for publication.

3. Software Development

We have spent a great deal of effort developing software for psychophysical experimentation. Thus, we also describe the developments that occurred during the grant period. These include development of specialized computer graphics programs, optimized rendering engines and tools needed to generate displays with specific spatial and temporal properties. Stereo 3D, texture mapping, high frame rate animation and real-time digital image manipulations. We have also developed a suite of external device control routines, sensor and actuator interfaces, drivers, control

algorithms, feedback loop systems (human motor through computer sensory channels) and low-level video synchronization tools necessary for doing real-time psychophysics experiments. Almost all the tools we are developing are in form of MATLAB shared libraries, external C or assembly programs interfaced to and called from MATLAB. This scheme allows us to tap into powerful high-level programming and analysis features of MATLAB while we implement experiments that require our low-level tools for doing real-time operations. All of our software tools are made available to the public through the Bankslab web page (http://john.berkeley.edu/software.html). They are currently used by many labs around the world. (See list below).

BitmapTools

BitmapTools is an external MATLAB plugin for generating high-frame rate animations (highest refresh rate possible on the graphics card/monitor). It allows for design and display of both static bitmaps and bitmap movies on Macintosh and Windows NT platforms. BitmapTools is designed around one important premise, to maximize the blitting (RAM to Video Memory transfer) rate. On the Macintosh, BitmapTools takes advantage of PowerPC processor's pipelining architecture through assembly level tweakings. On the PC (NT), high-bandwidth blitting is achieved through hardware-accelerated calls (DirectDraw). Almost all modern graphics cards contain the necessary hardware for BitmapTools. The issue with movie players in general is the unreliable animation frame rate. In BitmapTools, real-time frame rate is guaranteed. Under normal operations (on NT, with no major background processes), a 1024x768 movie can play at 120 hz without missing frames. If a frame is missed for some reason, exact location of the frame(s) in the sequence is reported.

OpenGLTools

OpenGLTools is a MATLAB external shared library (compiled mex file) that incorporates interactive 2D/3D graphics functionality into MATLAB. The main objective is to bridge MATLAB's high-level programming environment with the low-level OpenGL graphics engine. This is useful because MATLAB's data types and syntax are most natural for creation of basic 3D constructs, as well as hierarchical development and manipulation of the more complex graphics objects. OpenGLTools is augmented by a rich collection of operators and functions (toolboxes) embedded in MATLAB. It is designed as a research tool for vision scientists to create interactive visual stimuli with precise control over spatial, luminance and temporal properties. Some of the advanced features include stereo (anaglyph and LCD shutter glasses), texture mapping, lighting, buffer manipulations, image processing filters, and re-programmable interactive mouse bindings. OpenGLTools is available on MacOS, Windows, and Unix (IRIX), although Windows (NT) is the best supported platform.

FlightTools

FlightTools is a flight simulation construction plugin for MATLAB. Like OpenGLTools, it takes advantage of hardware-accelerated OpenGLTools calls. The user can define scene elements in form of MATLAB matrices and lists and specify a flight path and camera gaze lists. Real-time animation of flight allows interactive control of flight parameters such as pitch, yaw and roll control as well as other parameters used in construction of specific simulation functions.

SerialTools

Macintosh serial port communication driver code with an interface to MATLAB.

DAQTools

PPC, analog IO code for acquiring external analog signals via the card inside the PC. Implemented features include highest level synchronization of internal machine processes with independent data acquisition and processing events that take place in the IO card. Synchronized signal sampling and generation.

RemoteDAQ Tools

A remote data acquisition system, allowing a Macintosh to tap over the serial lines, into Data acquisition functions of an IO card housed on a host computer. It implements low-level synchronization features for guaranteeing synchronization of internal processes in the client machine with various data acquisition functions of the IO card on the remote host machine (ex: synchronization of the vertical video blanking signal on the client with the signal sampling process on the remote host computer housing the signal acquisition hardware). To give you an idea on the effectiveness of this tool, it was the basis for our VEP signal acquisition and processing system now used by Dr. Catherine Suttle in her VEP project at the University of Sydney. It implements the same fundamental functionality of the well-known VEP system that took Smith Kettlewell a number of years to develop.

4. Publications during Grant Period

Referred Journals

1. Backus, B.T. & Banks, M.S. (1999) Estimator reliability and distance scaling in stereoscopic slant perception. *Perception*, **28**, 217–242.

2. Backus, B.T., Banks, M.S., van Ee, R., & Crowell, J.A. (1999) Horizontal and vertical disparity, eye position and stereoscopic slant perception. *Vision Research*, **39**, 1143-1170.
3. Banks, M.S. & Backus, B.T. (1998) Extra-retinal and perspective cues explain the small range of the induced effect. *Vision Research*, **38**, 187–194.
4. Crowell, J.A., Banks, M.S., Shenoy, K.V., & Andersen, R.A. (1998) Visual self-motion perception during head turns is mediated by a non-linear interaction between three extra-retinal cues. *Nature Neuroscience*, **1**, 732-737.
5. Ehrlich, S.M., Beck, D., Backus, B.T., Crowell, J.A., & Banks, M.S. (1998) Depth information and the perception of heading. *Vision Research*, **38**, 3129-3146.
6. Ernst, M.O., Banks, M.S., & Bülthoff, H.H. (2000). Touch can change visual slant perception. *Nature Neuroscience*, **3**, 69-73.
7. Freeman, T.C.A. (1999). Path perception and Filehne illusion compared: model and data. *Vision Research*, **39**, 2659-2667.
8. Freeman, T.C.A. & Banks, M.S. (1998) Perceived speed during eye movements is affected by both extra-retinal and retinal errors. *Vision Research*, **38**, 941-946.
9. Freeman, T.C.A. Crowell, J.A. & Banks, M.S. (1999) Extra-retinal and retinal amplitude and phase errors during Filehne illusion and path perception. *Perception & Psychophysics*, in press.
10. van Ee, R., Banks, M.S., & Backus, B.T. (1999). An analysis of binocular slant contrast. *Perception*, **28**, 1121-1145.
11. van Ee, R., Banks, M.S., & Backus, B.T. (1999). Perceived visual direction near an occluder. *Vision Research*, **39**, 4085-4097.

Chapters.

12. Banks, M.S. & Backus, B.T. (1998) Use of horizontal disparity, vertical disparity, and eye position in slant perception. In L. Harris (ed.), *Vision and Action*. Oxford University Press.

Manuscripts under Review or in Preparation

13. Adams, W.J. Adams, Banks, M.S., & van Ee, R. (2000) Adaptation to 3d distortions in human vision. *Nature Neuroscience*, in revision.
14. Banks, M. S., Hooge, I. T. C., & Backus, B. T. (2000) Horizontal and vertical disparities, torsion signals, and perception of inclined surfaces. *Vision Research*.
15. Domini, F., Adams, W.J., & Banks, M.S. (2000) 3d aftereffects are due to shape and not disparity adaptation. *Vision Research*, in revision.
16. James, F.M.K., Humphrey, G.K., Banks, M.S., & Vilis, T. (2000). Accurate slant judgements bsed on extra-retinal eye position, *Vision Research*, in preparation.
17. Hillis, J.M. & Banks, M.S. (2000). Are corresponding points fixed? *Vision Research*, in preparation.
18. Hooge, I.T.C., Banks, M.S., & van den Berg, A.V. (2000). Subjective and objective measures of cyclovergence. *Vision Research*, in preparation.

5. Service for Air Force

During the grant period, the PI was asked to do a few things that might potentially benefit the Air Force.

In 1998, he traveled to Williams AFB in Arizona in order to meet with Byron Pierce and George Geri. During that trip, he consulted with Drs. Pierce and Geri on their ongoing research and discussed possible collaborations between the Berkeley and Williams' labs. This led to an equipment loan in which Williams sent us an SGI Crimson workstation and a Sony CRT projector.

In 2000, the PI was asked to join a team that would put together a research plan for the Spatial Disorientation Program for the Air Force Research Labs. This work consisted of reviewing the previous research plans, evaluating a plan written by investigators at Wright-Patterson AFB, and then traveling to Brooks AFB for a two-day meeting chaired by Bill Ercoline. The outcome was a 5-year research plan that is currently being evaluated by the Air Force.

In 2000, the PI participated in the Civic Outreach Program for two days. He traveled to Moffett Airfield, Edwards AFB, Cheyenne Mountain, and Peterson AFB and participated in briefings, tours, and discussions with Air Force personnel.

6. Significance of Research Program for Air Force

During the past grant period, we examined visual navigation and space perception in humans. We believe that our research is highly relevant to the military aviation mission. The main area of Air Force need that is addressed by our research is spatial disorientation (SD) and the use of synthetic or enhanced visual display devices such as head-mounted displays (HMDs), night-vision goggles (NVGs), the advanced aircraft control station (ACS), and more.

SD remains a major safety problem in flight and SD is likely to become an even more serious problem as the

next wave of aircraft (e.g., agile flight) is developed and put into flight. Our work on heading perception is aimed at determining the complex of visual and non-visual signals that are used to estimate the direction of self-motion and ones orientation with respect to gravity. Specifically, we are working on determining how much weight is given to various signals (e.g., optic flow vs vestibular) and how those weights depend on the viewing situation (e.g., weight given to vestibular increases as the optic flow information is degraded). With a better understanding of how the human nervous system computes and weights these various sources of information we will be able to provide the Air Force material relevant to pilot training, cockpit design, and the configuration of synthetic visual displays. Let us give one specific example. In our work on the somatogravic ("pitch up") illusion, we are trying to determine what visual cues must be present in order to override the vestibular-based illusion of upward pitch. Once we know what the critical visual cues are, we can recommend the design of an artificial cockpit display (e.g., an artificial horizon) that would minimize the illusion.

Our work on space perception, primarily slant and curvature perception, is also quite relevant to the military aviation mission. In the next generation of military aircraft, we will see greater and greater reliance on synthetic visual displays. Indeed, if the closed cockpit (all virtual) aircraft is brought on line, all of the visual information provided to the pilot will be synthetic. We have found that perceived depth is based on the integration of numerous visual (e.g., disparity and texture gradient) and non-visual (e.g., eye muscle signals) cues. The final percept is the result of a weighted combination of those various cues. An understanding of how those cues are calculated and weighted in the nervous system is critical to the design of a synthetic visual display. For example, we know from our work that cues provided by the CRT itself (e.g., pixelization, focus cues) cause perceptual depth compression. Such compression would be highly undesirable in an all-virtual cockpit and so the design of the visual display will either have to reduce the influence of such competing cues or figure out how to override them.

Finally, our software development might also be quite useful to the Air Force. At a meeting at Brooks AFB in March, 2000 (chaired by Bill Ercoline), a potential business plan was formed for the next 5 years. One idea presented in this plan was to generate web-based instructional aides for teaching spatial disorientation to future pilots. One of our software developments – FlightTools – would allow us to recreate flight scenarios that could be played on the internet for use in the classroom. Those scenarios could be seen from the perspective of the pilot or from an outside perspective (chosen by the student). The scenarios can be produced on standard PCs with off-the-shelf video cards. The Banks Lab is committed through its relationship with the Air Force to produce material like this whenever it might be needed.

7. Literature Cited

Backus, B. T. & Banks, M. S. (1999). Estimator reliability and distance scaling in stereoscopic slant perception. *Perception*, 28, 217-242.

Backus, B. T., Banks, M. S., van Ee, R. & Crowell, J. A. (1999). Horizontal and vertical disparity, eye position, and stereoscopic slant perception. *Vision Research*, 39, 1143-1170.

Banks, M. S. & Backus, B. T. (1998a). Extra-retinal and perspective cues cause the small range of the induced effect. *Vision Research*, 38, 187-194.

Banks, M. S. & Backus, B. T. (1998b) Use of horizontal disparity, vertical disparity, and eye position in slant perception. In L. Harris (ed.), *Vision and Action*. Oxford University Press.

Banks, M. S., Ehrlich, S.M., Backus, B.T., & Crowell, J.A. (1996). Estimating heading during real and simulated eye movements. *Vision Research*, 36, 431-443.

Banks, M. S., Backus, B. T., Hooge, I.T.C., & van den Berg, A.V. (1999). Horizontal and vertical disparities, torsion signals, and perception of inclined surfaces. *ARVO*.

Banks, M. S., Hooge, I. T. C., & Backus, B. T. (2000) Horizontal and vertical disparities, torsion signals, and perception of inclined surfaces. *Vision Research*, in preparation

Brookes, A. & Stevens, K.A. (1989). The analogy between stereo depth and brightness. *Perception*, 18, 601-614.

Buckley, D. & Frisby, J. P. (1993). Interaction of stereo, texture and outline cues in the shape perception of three-dimensional ridges. *Vision Research*, 33, 919-33.

Clarke, J. J. & Yuille, A.L. (1990). *Data Fusion for Sensory Information Processing Systems*. Boston : Kluwer.

Crowell, J. A., Banks, M.S., Shenoy, K.V., & Andersen, R.A. (1998). Visual self-motion perception during head turns. *Nature Neuroscience*, 1, 732-737.

Cumming, B. G., Johnston, E. B., & Parker, A. J. (1993). Effects of different texture cues on curved surfaces viewed stereoscopically. *Vision Research*, 33, 827-38.

Cutting, J. E. & Millard, R. T. (1984). Three gradients and the perception of flat and curved surfaces. *Journal of Experimental Psychology: General*, **113**, 198-216.

Ehrlich, S.M., Beck, D.M., Crowell, J.A., Freeman, T.C.A., & Banks, M.S. (1998). Depth information and perceived self-motion during simulated gaze rotations. *Vision Research*, **38**, 3129-3145.

Ernst, M.O., Banks, M.S., & Bültholff, H.H. (1999) Touch can change visual slant perception. *Nature Neuroscience*, **3**, 69-73.

Fahle, M. & Westheimer, G. (1988). Local and global factors in disparity detection of rows of points. *Vision Research*, **28**, 171-178.

Foley, J. M. (1980). Binocular distance perception. *Psychological Review*, **87**, 411–34.

Freeman, T.C.A. (1999). Path perception and Filehne illusion compared: model and data. *Vision Research*, **39**, 2659-2667.

Freeman, T.C.A. & Banks, M. S. (1998). Perceived head-centric speed is affected by both extra-retinal and retinal errors. *Vision Research*, **38**, 941-945.

Freeman, T.C.A., Crowell, J.A., & Banks, M.S. (2000). Errors in path perception during gaze rotation. *Perception & Psychophysics*, in press.

Garding, J., Porrill, J., Mayhew, J. E., & Frisby, J. P. (1995) Stereopsis, vertical disparity and relief transformations. *Vision Research*, **35**, 703-722.

Gibson, J. J., Olum, P., & Rosenblatt, F. (1955). Parallax and perspective during aircraft landings. *American Journal of Psychology*, **68**, 373-385.

Gillam, B. & Lawergren, B. (1983). The induced effect, vertical disparity, and stereoscopic theory. *Perception and Psychophysics*, **34**, 121–30.

Gillam, B. & Ryan, C. (1992). Perspective, orientation disparity, and anisotropy in stereoscopic slant perception. *Perception*, **21**, 427-39.

Gillam, B., Chambers, D., & Lawergren, B. (1988). The role of vertical disparity in the scaling of stereoscopic depth perception: An empirical and theoretical study. *Perception and Psychophysics*, **40**, 477–83.

Gogel, W.C. (1956). The tendency to see objects as equidistant and its inverse relation to lateral separation. *Psychological Monographs*, **70**, 1-17.

Graham, M.E. & Rogers, B.J. (1982). Simultaneous and successive contrast effects in the perception of depth from motion-parallax and stereoscopic information. *Perception*, **11**, 247-262.

Harker, G.S. (1962). Apparent frontoparallel plane, stereoscopic correspondence, and induced cyclorotation of the eyes. *Perceptual and Motor Skills*, **14**, 75-87.

Harris, C.S. (1980). Perceptual adaptation to inverted, reversed, and displaced vision. *Psychological Reviews*, **72**, 419-444.

Heller, L. M. & Trahiotis, C. (1996) Extents of laterality and binaural interference effects. *Journal of the Acoustical Society of America*, **99**, 3632-3637.

Hooge, I.T.C., Banks, M.S., & van den Berg, A.V. (2000). Subjective and objective measures of cyclovergence. *Vision Research*, in preparation.

Howard, I. P. & Kaneko, H. (1994). Relative shear disparities and the perception of surface inclination. *Vision Research*, **34**, 2505-17.

Howard, I. P. & Rogers, B.J. (1995). *Binocular vision and stereopsis*. New York: Oxford Press.

Howard, I. P., Ohmi, M., & Sun, L. (1993). Cyclovergence: A comparison of objective and psychophysical measurements. *Experimental Brain Research*, **97**, 349-355.

Howard, I. P. (1982). *Human spatial orientation*. Chichester: Wiley.

James, F.M.K., Humphrey, G.K., Banks, M.S., & Vilis, T. (2000). Accurate slant judgements bsed on extra-retinal eye position. *ARVO* presentation.

Kaneko, H. & Howard, I. P. (1996). Relative size disparities and the perception of surface slant. *Vision Research*, **36**, 1919-1930.

Koenderink, J. J. & van Doorn, A. J. (1976). Geometry of binocular vision and a model for stereopsis. *Biological Cybernetics*, **21**, 29–35.

Landy, M. S., Maloney, L. T., Johnston, E. B. & Young, M. (1995). Measurement and modeling of depth cue combination: in defense of weak fusion. *Vision Research*, **35**, 389-412.

Longuet–Higgins, H. C. (1982). The role of the vertical dimension in stereoscopic vision. *Perception*, **11**, 371–6.

Mack, A. & Herman, E. (1973). Position constancy during pursuit eye movements: an investigation of the Filehne illusion. *Journal of Experimental Psychology*, **25**, 71-84.

Mack, A. & Herman, E. (1978). The loss of position constancy during pursuit eye movements. *Vision Research*, **18**, 55-62.

Mayhew, J. E. W. & Longuet–Higgins, H. C. (1982). A computational model of binocular depth perception. *Nature*, **297**, 376–8.

Mitchison, G. J. and McKee, S. P. (1990). Mechanisms underlying the anisotropy of stereoscopic tilt perception. *Vision Research*, **30**, 1781–91.

Nakayama, K. & Balliet, R. (1977). Listing's Law, eye position sense, and perception of the vertical. *Vision Research*, **27**, 453-457.

Nelson, J. (1977). The plasticity of correspondence: after-effects, illusions and horopter shifts in depth perception. *Journal of Theoretical Biology*, **66**, 203-266.

Ogle, K. N. (1938). Induced size effect. I. A new phenomenon in binocular space–perception associated with the relative sizes of the images of the two eyes. *AMA Archives of Ophthalmology*, **20**, 604–23.

Ogle, K. N. (1946). The binocular depth contrast phenomenon. *American Journal of Psychology*, **59**, 111-126.

Ogle, K. N. (1950). *Researches in binocular vision*. Hafner, New York.

Pastore, N. & Terwilliger, M. (1966). Induction of stereoscopic depth effects. *British Journal of Psychology*, **57**, 201-202.

Pastore, N. (1964). Induction of stereoscopic depth effect. *Science*, **144**, 888.

Pierce, B.J., Howard, I.P., & Feresin, C. (1998). Depth interactions between inclined and slanted surfaces in vertical and horizontal orientations. *Perception*, **27**, 87-103.

Poggio, T., Gamble, E.B., & Little, J.J. (1998). Parallel integration of vision modules. *Science*, **242**, 436-439.

Rogers, B. J. & Bradshaw, M. F. (1993). Vertical disparities, differential perspective and binocular stereopsis. *Nature*, **361**, 253–255.

Rogers, B. J. & Bradshaw, M. (1995). Disparity scaling and the perception of frontoparallel surfaces. *Perception*, **24**, 155-179.

Rogers, B. J. & Graham, M. E. (1983). Anisotropies in the perception of three–dimensional surfaces. *Science*, **221**, 1409–1411.

Royden, C.S., Banks, M.S., & Crowell, J.A. (1992). The perception of heading during eye movements. *Nature*, **360**, 583-585.

Royden, C.S., Crowell, J.A., & Banks, M.S. (1994). Estimating heading during eye movements. *Vision Research*, **34**, 3197-3214.

Royden, C.S. (1994). Analysis of misperceived observer motion during simulated eye rotations. *Vision Research*, **34**, 3215-3222.

Sedgwick, H. A. (1986). Space perception. *In Handbook of human perception and performance*, (ed. K. R. Boff, L Kaufman, & J. P. Thomas), Chap. 21. Wiley, New York.

Sibigtroth, M.P. & Banks, M.S. (2000). Perspective transformation in heading estimation. *ARVO* presentation.

Stevens, K. A. & Brookes, A. (1988). Integrating stereopsis with monocular interpretations of planar surfaces. *Vision Research*, **28**, 371-386.

van den Berg, A.V. & Brenner, E. (1994). Humans combine the optic flow with static depth cues for robust perception of heading. *Vision Research*,**34**, 2153-2167.

van den Berg, A.V. (1996). Judgments of heading. *Vision Research*, **36**, 2237-2350.

van Ee, R. & Erkelens, C. J. (1996). Anisotropy in Werner's binocular depth contrast effect. *Vision Research*, **36**, 2253-2262.

van Ee, R., Banks, M. S., & Backus, B. T. (1999). An analysis of binocular slant contrast. *Perception*, **28**, 1121-1145.

van Ee, R. (1995). *Stability of binocular depth perception*. Utrecht: Utrecht University.

Warren, W.H., Morris, M.W., & Kalish, M. (1988). Perception of translational heading from optical flow. *Journal of Experimental Psychology*, **17**, 28-43.

Welch, R.B. (1986). *Perceptual modification: Adapting to altered sensory environments*. New York: Academic.

Werner, H. (1937). Dynamical theory of depth perception. *Psychological Monographs*, **49**, 1-127.

Werner, H. (1938). Binocular depth-contrsadt and the conditions of the binocular field. *American Journal of Psychology*, **51**, 489-497.

Wertheim, A.H. (1987). Motion perception during self-motion-the direct versus inferential controversy revisited. *Behavioural and Brain Sciences*, **17**, 293-311.

Yasui, S. & Young, L.R. (1975). Perceived visual motion as effective stimulus to pursuit eye movement system. *Science*, **190**, 906-908.